2

Conf-940142--33

UCRL-JC-116059
PREPRINT

Improved Performance of High Average Power Semiconductor Arrays for Applications in Diode Pumped Solid State Lasers

R. Beach, M. Emanuel, W. Benett, B. Freitas, D. Ciarlo,
N. Carlson, S. Sutton, J. Skidmore, R. Solarz

This paper was prepared for submittal to the
Laser Diode Technology and Applications VI-SPIE OE/LASE '94
Los Angeles, CA
January 22-29, 1994

January, 1994

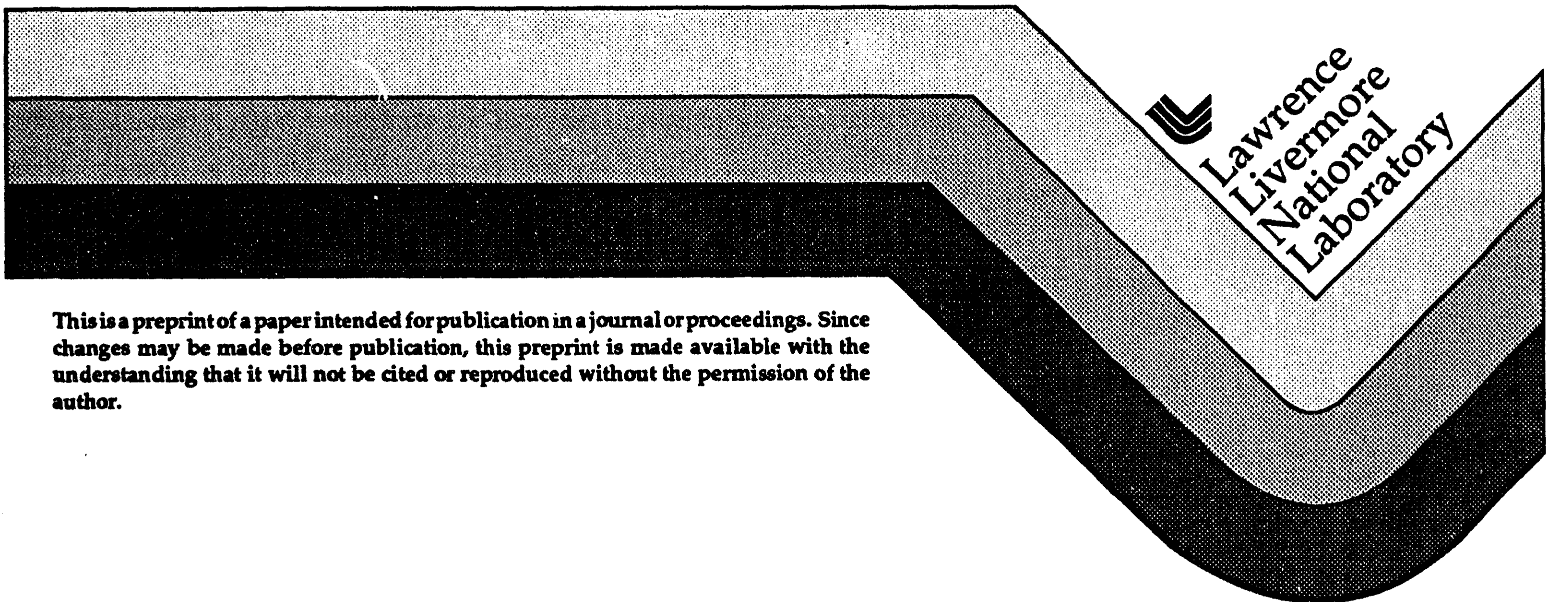

This is a preprint of a paper intended for publication in a journal or proceedings. Since changes may be made before publication, this preprint is made available with the understanding that it will not be cited or reproduced without the permission of the author.

MASTER

DISTRIBUTION OF THIS DOCUMENT IS UNLIMITED

DISCLAIMER

This document was prepared as an account of work sponsored by an agency of the United States Government. Neither the United States Government nor the University of California nor any of their employees, makes any warranty, express or implied, or assumes any legal liability or responsibility for the accuracy, completeness, or usefulness of any information, apparatus, product, or process disclosed, or represents that its use would not infringe privately owned rights. Reference herein to any specific commercial products, process, or service by trade name, trademark, manufacturer, or otherwise, does not necessarily constitute or imply its endorsement, recommendation, or favoring by the United States Government or the University of California. The views and opinions of authors expressed herein do not necessarily state or reflect those of the United States Government or the University of California, and shall not be used for advertising or product endorsement purposes.

SPIE94.DOC January 5, 1994

Improved Performance of High Average Power Semiconductor Arrays for Applications in Diode Pumped Solid State Lasers

Ray Beach, Mark Emanuel, William Benett, Barry Freitas, Dino Ciarlo
Nils Carlson, Steve Sutton, Jay Skidmore, Richard Solarz

Lawrence Livermore National Laboratory
PO Box 808, L-495
Livermore, California 94550

RECEIVED
APR 13 1994
OSTI

Abstract

The average power performance capability of semiconductor diode laser arrays has improved dramatically over the past several years. These performance improvements, combined with cost reductions pursued by LLNL and others in the fabrication and packaging of diode lasers, have continued to reduce the price per average watt of laser diode radiation. Presently, we are at the point where the manufacturers of commercial high average power solid state laser systems used in material processing applications can now seriously consider the replacement of their flashlamp pumps with laser diode pump sources. Additionally, a low cost technique developed and demonstrated at LLNL for optically conditioning the output radiation of diode laser arrays has enabled a new and scalable average power diode-end-pumping architecture that can be simply implemented in diode pumped solid state laser systems (DPSSL's). This development allows the high average power DPSSL designer to look beyond the Nd ion for the first time. Along with high average power DPSSL's which are appropriate for material processing applications, low and intermediate average power DPSSL's are now realizable at low enough costs to be attractive for use in many medical, electronic, and lithographic applications.

Introduction

The type of packaging technology applied to semiconductor laser diode arrays is key to enabling the high average power performance of these devices. Not only must the laser diode package be capable of efficiently shedding the large heat intensities generated at the laser diode array with only a small temperature rise at the device, it must also be low cost to implement if it is to be attractive to commercial users. In designing the LLNL laser diode package these points were seriously addressed and a systems level approach was used in carrying out the design. The laser diode packaging group worked closely with the solid state laser design groups at LLNL to develop a package that would be suitable to applications involving the diode pumping of high average power solid state laser systems. In addition to the requirements of aggressive heatsinking and low cost, the package was also required to be modular and to minimize the number of external hydraulic and electrical connections to the large two dimensional arrays that were to be constructed using many of the modular packages. The modularity of the package was required to ensure maintainability of large two-dimensional arrays. It was desired to hold the level of diode array integration to several linear centimeters of diode array bar length per package so that if it became necessary to service a large array, small sections could be replaced cheaply and easily. Minimizing the number of external hydraulic connections to large arrays constructed from the LLNL package was necessary to ensure the simple and flexible implementation of these arrays into DPSSL systems in which the number of external hydraulic connections to the diode pumps impacts system complexity as well as the overall system size and weight. In many of the military systems LLNL is involved in, weight and volume envelopes are often the deciding factor as to a system's viability for its intended mission. In commercial systems; it is the simplicity, improved maintainability, and cost savings that can be realized when the hydraulic circuits are simplified that is attractive. To ensure the packaging manufacture technology was low cost in terms of its implementation and consumed materials a silicon based packaging technique was chosen. As explained below no exotic, expensive, high thermal conductivity materials (such as synthetic diamond) are used in the package; it is fabricated entirely from silicon and borosilicate glass.

Package Description

Figure 1 is a photograph of the present version of the LLNL laser diode package. Because it has been previously described elsewhere[1 2]only a brief overview will be given here. The approximate package dimensions are 2 cm x 2 cm x 0.75 mm thick. The package can hold up to 1.8 linear cm of bar material visible underneath the wire bonds along the top edge of the photo. The circular holes on the right hand side of the package are internally connected and serve as the water inlet. Similarly, the holes on the left of the package are internally connected and serve as the water outlet. The central hexagonal hole is for a bolt allowing the modules to be stacked to make two-dimensional arrays. The metallization pad visible in the photograph to which the wire bonds are attached serves as the electrical n-side diode contact. The diode bar is mounted p-side down on a metal pad

that runs along the top edge of the package and then wraps around and connects to the bottom of the package (not visible in the photograph) which serves as the p-side contact.

Figure 2a shows the laminated structure of the package in an exploded view. Two layers of silicon and one layer of borosilicate glass are used in the fabrication of the package. The borosilicate glass insert is sandwiched between the two pieces of etched silicon which comprise the manifold layer and the microchannel layer. All features on the glass piece are through-holes. On the silicon pieces the central and four outlying holes are through-holes while the remaining patterned features are etched to a depth of approximately 150 microns. The sides of the silicon pieces not shown are featureless except for the through-holes and the canted front edge of the package. Figure 2b is a cross-sectional view of the three layers showing the water flow path and the package's canted front edge. Each silicon layer is approximately 250 microns thick as is the central glass layer. The purpose of the etched features in the silicon bottom layer is to convert the flow of inlet cooling water which enters the package through the two holes on the right hand side of Fig. 2a into sheet flow toward the front of the package. Once at the front of the package the water is turned toward the top layer of silicon through a slot that is ultrasonically milled into the central glass layer. After exiting the slot, the water enters the microchanneled region directly below the location of the diode bar. The scanning electron microscope photograph of a cut away package in Fig. 3 shows these microchannels. The channels are approximately 150 microns deep and 25 microns wide and 2 mm long. Continuing, the water exits the microchannels and enters a sheet flow region in the top layer of silicon where it is directed back to the outlet holes on the left side of Fig 2a. The purpose of the canted front edge of the package (visible in Fig 2b) which falls away from the horizontal at an angle of 35.3° is to allow the laser light that is emitted by the diode to clear the package without having to reflect off any surfaces. As will be discussed later this cant feature is also critical for allowing the optical conditioning of the emitted laser light.

The microchannel features in Fig. 3 are responsible for the aggressive cooling capability of the LLNL package. In flowing liquid coolant loops, such as the one used in the LLNL package, it is generally true that the thermal bottleneck or the highest temperature rises are incurred in the stagnant fluid boundary layer that is always present between a flowing liquid and a solid. The source of these stagnant boundary layers is the no slip boundary condition that exists at such interfaces. It is easy to see that these stagnant boundary layers are the big lever in controlling the temperature rise in a thermal circuit when one realizes that the thermal conductivity of typical solids used in heatsinks is many times larger than the thermal conductivity of the typical fluids that flow through them. For example, the thermal conductivity of the silicon used in the LLNL package at 1.5 W/cm-°C is 250 times larger than that of water at 0.0061 W/cm-°C. To minimize thermal boundary layer temperature rises two competing techniques have been developed. One of these techniques makes use of high Reynolds number turbulent flow such as used in the compact high intensity cooler (CHIC)[3], the other makes use of laminar flow through microchannels[4] and is the approach we have adopted. The simplest way to view how microchannels drive down the boundary layer thickness is to note that as long as fluid is being forced through the channels, the boundary layer cannot be any thicker than half the

channel width. This explains the use of the narrow channel, as the boundary layer width scales with the physical channel width. One advantage of the microchannel approach over the CHIC approach is that the microchannels are very efficient in terms of their consumed hydraulic power because they use low Reynolds number laminar flow. This is in contrast to the turbulent flow used in the CHIC approach which generally requires higher flow velocities and larger pressure drops to achieve heat transfer coefficients comparable to those realized in the microchannel approach. The interested reader is referred to the excellent treatments in the literature that discuss the heat transfer physics and design optimization procedures for microchannel coolers.[5] [6]

Package Fabrication

Because it was already previously well developed, low cost to implement, and leads to an inexpensive manufacturing process, a silicon based fabrication technology was chosen for the LLNL package. Figure 4 shows a drawing of the patterned silicon layers used for the top microchannel and bottom manifold layer of the package and the glass insert used as the central layer. Presently we are using a 3" silicon wafer technology that allows six individual patterns to be etched on each wafer piece as shown in Fig. 4. The approximate thicknesses of the silicon wafers and the central glass insert are 250 microns. The silicon wafers are (110) oriented; this allows the through holes, manifold features, microchannels, and canted front edge feature to be anisotropically etched in a single step. In this etching process an 800 Angstrom SiN layer is deposited on both wafer surfaces and appropriately patterned using a photolithographic process to define those areas that are to be etched. The wafers are etched in a 44% KOH solution for a predetermined time. The approximate etch rate is 4 microns/hour with the exact rate being dependent on the feature size being etched. The central glass insert is fabricated using an ultrasonic machining technique. The three wafer layers shown in Fig. 4 are joined using an anodic bonding procedure[7]. In this process the three layers are placed in contact with each other and heated in an oven to 560 °C, the annealing temperature of the borosilicate glass insert. Using the glass as a negative electrode and the two silicon layers as positive electrodes, an increasing voltage difference is applied, up to 500 V, over a period of 45 minutes. The electrostatic force pulls the glass and silicon into intimate contact, forming a very strong bond at the interface. After the bonding is completed, the parts are annealed at high temperature for approximately 2 hours before being removed from the oven. After cooling, the wafer assemblies are cut into individual packages using a dicing saw.

Industry standard thin film metallizations are applied to the coolers using a shadow masking technology. Starting at the silicon and going out the metallization layers are 1000 Å of Ti, 400 μm of Au, 1000 Å of Pt, and 1000 Å of Au. The thick Au ensures a low resistance current path for the up to 250 amps of current that run through the packages. As already discussed the package is metallized on its top, bottom and front edge, with a break in the metallization that runs just below the diode bar. This break is located just underneath the wire bonds in Fig. 1 and provides isolation for the n-side contact to which the wire bonds are attached. The diode bar is soldered to the package using a 3 μm thick layer of indium that is deposited by evaporation. The final step in the package production

is the wire bonding from the n-side of the bar to the packages n-side contact. This is accomplished using approximately 200, 1.25-mil-diameter Au wires.

Large Stack Fabrication

Figure 5a shows a LLNL package along with a matching conductive silicone elastomer gasket. The gasket, which is 250 μm thick and has the same hole pattern as the package, is placed directly over the package making a stackable module which is the unit cell of larger stacks. Such package-gasket assemblies are ganged one on top of another using the central hole to locate on a screw as shown in Fig. 5b. The overall thickness of such package-gasket assemblies is 1 mm , yielding a stacking pitch of 10 packages per cm. Using this stacking procedure, arbitrarily large two-dimensional apertures can be constructed. The central locating screw is used to hold the stack in compression when it is completed. In such stacks the conductive gaskets provide electrical continuity from package to package as well as hydraulic sealing between the packages. Regardless of the length of the stack, water connections from package to package are made automatically by the gaskets so that a finished stack simply has one water inlet and one water outlet. This feature greatly simplifies the integration of such large two-dimensional diode pump arrays into DPSSL systems and enhances the flexibility of the LLNL packaging approach.

Figure 6a is a photograph of a large 2-dimensional diode array used to pump a Nd:YAG slab laser. Figure 6b is a photograph of the Nd:YAG zigzag slab laser which is being developed at LLNL for applications in the generation of x-rays for a lithography application as well as material processing applications. The array in Fig. 6a was constructed by stacking 148 of the LLNL packages, The single screw that is used to hold this stack in compression is visible on the left hand side of the stack as are the two water connections on the back side of the array. Electrically, the packages in such stacks are connected in series resulting in a single positive and negative electrode at either end of the stack. One advantage of the stacking technology developed by LLNL is the ease it brings to the maintenance of such large arrays. If for some reason it becomes necessary to replace a package it is a simple matter to remove the compressing screw, remove a single package, replace it with another one, and then reassemble the stack.

Package Performance

Figure 7 plots the average power capability of laser diode bars normalized to a 1 cm bar length that has been demonstrated over the past 4 years using the LLNL silicon microchannel cooled package. The improvements in performance over the past several years are due both to the continuing improvements in the quality of laser diode array bar material and improvements made to the microchannel coolers themselves. Figure 8 plots the cw optical power from an LLNL package containing a 1 cm long fully filled laser diode bar (100 micron wide stripes on 140 micron centers) with a 1 mm cavity length. This 808 nm bar which was fabricated at LLNL from epi material grown at LLNL was operated cw to an output power of 96 W without exhibiting any signs of thermal roll over

or damage. This demonstrated average power capability and the present package stacking pitch of 10/cm leads to stack irradiances of 960 W/cm^2.

One of the critical factors to obtaining reliable performance from high average power laser diode arrays involves minimizing the degradation that occurs in the thermal circuit which removes the waste heat generated by the diode bar. If this thermal circuit degrades the bar will run hotter which adversely impacts both the performance and reliability of the diode. In the design of the LLNL package these considerations led us to limit the number of solder interfaces between the laser diode bar and the cooling water to one because it is generally at such solder interfaces between dissimilar materials that the thermal impedance degrades over time. This is in contrast to the diode packaging widely used in the commercial arena now where two or three solder joints are typically placed between the laser diode bar and the cooling water.[8] The criticality of the solder interfaces can be appreciated by considering the 1 cm long by 1 mm cavity length bar used to generate the data in Fig. 8. If this bar is running at a cw output of 100 W with a 50% efficiency the thermal intensity at the footprint of the bar is 1 KW/cm^2. Typical thermal engineering problems in which such high thermal intensities are encountered are in the design of rocket nozzle throats and heat shields for ballistic entry; situations in which acceptable temperature rises can be several thousand degrees centigrade. In the case of cooling laser diode arrays, these same thermal intensities must be handled but now the acceptable temperature rise is only several tens of degrees centigrade. This places very stringent requirements on both the uniformity and reliability of the solder interface between the diode bar and the cooler. The same considerations also point to keeping the thermal circuit as nple as possible; the more solder interfaces there are the more places the thermal . ıcuit can degrade.

It has already been mentioned that one of the advantages of the microchannel cooling approach over other competing technologies is that it is very efficient in terms of its consumed hydraulic power. In high average power applications such as the running of the device that generated the data in Fig. 8 the pressure drop across the packages was 50 PSI and the flow through the package was approximately 2 cm^3/sec. This represents a consumed hydraulic power of 0.7 W for a packaged device that is capable of generating 100 W of cw optical output. In the design of the LLNL package there was a trade off between consumed hydraulic power and overall package thermal impedance that had to be balanced. This happens because essentially all of the pressure drop occurs through the microchannel region of the package and so hydraulic power consumption can be decreased by design through the opening up of the microchannel dimensions. However, this opening up of the channel dimensions increases the thermal boundary layer component of the package's thermal impedance and so increases the overall temperature at which the diode bar runs. In the design of the LLNL package it was decided to size the microchannels such that the consumed hydraulic power would be 1% or less of the optical output power capability of the package.

Figure 9 displays the results of a constant light output lifetest in which a 1 cm bar was operated at 22.2 W cw by continually adjusting the drive current to hold the output power

constant. Based on the measured degradation rate over the first 1000 hours of operation the projected time lapse until the drive current is required to be increased by 30% over its initial value is 9000 hours (1 year). The time until a 30% increase in current is required is the useful lifetime we specify for the diode pumps in DPSSL systems that we constructed. The data in Fig. 8 was generated using 808 nm AlGaAs laser diode material from purchased from Siemens and represents the current state of the art in material that we procure from commercial companies. Because all of the degradation we observed took place in the diode bar itself, there was no degradation in the solder joint or the package's thermal impedance, this 9000 hours does not represent the ultimate lifetime of such high power cw devices. Based on literature reports, there should be substantial improvements in lifetimes in going to InAlGaAs diode laser arrays where it has been demonstrated that the degradation in performance due to dark line defects is substantially less than what is observed in AlGaAs.[9]

As mentioned earlier, past performance improvements have been due to continuing improvements in the quality of diode-laser array material and improvements made in the microchannel coolers. However, future performance improvements will depend critically on developing processes that will raise the power-density level where catastrophic facet damage occurs. As a graphic illustration of this, Figure 10 displays the theoretical maximum-power output of a 1 cm wide bar (with output facet reflectivity continually adjusted to provide maximum-extraction efficiency) versus cavity length for material losses of 5 cm^{-1} and 1 cm^{-1}, which are respectively representative of some of the higher and highest quality material available. These curves were calculated using a small-signal modal gain of 500 cm^{-1} and a saturation intensity of 0.5 MW/cm^2. Low loss material has a longer absorption length ($1/\alpha$) so it is possible to increase the cavity length, so that higher-power outputs are possible from a 1 cm bar, while maintaining a near-optimum energy-extraction efficiency. An additional benefit of using longer-cavity lengths is that a larger thermal-footprint is obtained, which reduces the heat dissipation per unit area. The horizontal line corresponds to the onset of catastrophic facet damage. Although operation in the vicinity or above this limit is certainly possible, as demonstrated on numerous occasions, reliable cw operation at 10,000 hrs at these elevated power levels (in the 100 W range) has not yet been achieved.

Also, indicated on the same plot (on the left axis in Fig. 10) is the maximum-thermal power that can be dissipated in a 1 cm bar and be removed with the current generation of silicon micro-channel coolers. For this thermal limit, the diode bars were assumed to be 50 % efficient and the heat-removal capacity of the silicon micro-channel coolers was 2 KW/cm^2. The line corresponds to a 28 °C temperature rise at the bar corresponding to a thermal impedance of 0.014 $°C\text{-}cm^2/W$. Note that the parameters used to construct this thermal limit are intentionally conservative to reflect the more demanding thermal-management requirements imposed by cw and high-average power operation. For short-pulsed operation at sufficiently low-duty cycle, heat dissipation is not a limiting factor; and in some operational scenarios, much higher temperature rises than 28 °C can be tolerated. One such example where this occurs is when the diode bars are fabricated using the InGaAs/GaAs material system. It is interesting to note that for cavity lengths > 0.8 mm

and cw output of ~200 W, the thermal limit crosses above the facet damage limit. This illustrates the necessity of raising the facet damage limit in order to obtain higher-power outputs and reliability from diode-pump arrays. Clearly, to operate with high reliability at or beyond the 100 W limit, the facet damage limit problem is the next obstacle that needs to be overcome. The final point here that needs to be emphasized is that, to the extent that the facet damage limit can be raised, or even eliminated, significant reductions in the cost per average Watt from diode-laser pump arrays are still possible.

Optical Conditioning and Scalable Diode End-Pumping Architecture

Because diode radiation is generated in a wave guide structure whose height is only slightly larger than the radiation's wavelength, the fast axis divergence angle of the radiation (the direction perpendicular to the p-n junction plane) can be as large as 60° (FWHM). For many applications requiring the concentration of pump radiation this is problematic because large two dimensional arrays do not allow efficient concentration in the fast axis direction without some type of optical conditioning to reduce the fast axis divergence. To address this problem LLNL has developed an inexpensive cylindrical microlens technology that allows the efficient collection and conditioning of the diode radiation in the fast axis direction.[10] Figure 11 shows a cross sectional view of an LLNL laser diode package with a conditioning microlens attached. Our latest generation microlens is shaped to rest on the canted front edge of the package in front of the laser diode bar with its flat surface toward the emitting diode. The lens collects the light emitted from the diode with up to a 60° (1 Rad) divergence angle and collimates it to approximately 0.6° (10 mRad). The usefulness of this technology is that now when large two-dimensional arrays are built by ganging packages one on top of another the effective radiance in the fast axis direction is increased by a factor of 100, effectively allowing large stacks to be focused down to spots in this fast axis dimension that are a factor of 100 smaller in spatial extent than they would have been had there been no optical conditioning performed.

Figure 12a depicts a scalable diode-end-pumping architecture that has been developed and demonstrated at LLNL in which a microlens conditioned stack of laser diode packages is used as the pump excitation source for a rod laser.[11] At the output end of the lensing duct, which is used to couple the microlens conditioned laser diode radiation to the laser rod, we have demonstrated pump intensities of 75 KW/cm^2. As a pump architecture, this ability to generate scalable high intensity pump radiation enables new applications for diode lasers that were previously not possible. LLNL has recently demonstrated an AlGaAs diode laser array pumped Cr:LiSAF laser[12] using this approach. Other applications requiring high intensity diode laser pumps such as bleach wave pumping[13] can now be realistically entertained in scalable systems. One of the very promising commercial developments to be emerging with this technology is in the area of high average power DPSSL systems for material processing applications in which a rod laser technology is pursued using Yb:YAG as the gain element.[14] The high intensities that can be generated with the LLNL end-pumping technology offer an opportunity to overcome the deleterious ground state re absorption problem of the Yb^{3-} ion. At the same time, advantage can be

taken of the very small thermal power generation parameter of the Yb^{3+} ion by using the high average power capability of the LLNL diode laser technology to implement a high average power DPSSL system using a very simple rod laser approach.

Figure 12b is a photograph of a microlens conditioned diode laser array and the lensing duct which is used to deliver the pump radiation to an output aperture which is square in shape and measures 2.2 mm on a side. The pump array in this case consists of 60 LLNL packages with each package carrying 1 linear cm of diode bar material. The lensing duct may be fabricated from any optical material transparent to the diode radiation. The material used for the lensing duct of Fig. 12b is fused silica and it was fabricated to LLNL's specifications by Lightning Optical Corporation. The output aperture of the lensing duct is square in cross section and is dimensioned such that it just inscribes the circular end of the laser rod that is being pumped by the diodes. The best way to visualize the operation of this optical element is to view it as an immersion lens with its output face located at its focus; ie, its length l, radius of curvature R, and index of refraction n are related by $l=R \cdot n/(n-l)$. In practice the output face is located before the focus, at the circle of least confusion to improve the transfer efficiency of the device. The purpose of the canted planar faces is deliver that pump light to the rod aperture by total internal reflection that would otherwise have fallen outside the input aperture of the laser rod.

Key to the end-pumping technology described here is the ability to inexpensively fabricate very fast cylindrical microlenses that efficiently collect the emitted diode radiation and then collimate it. At LLNL a technique has been demonstrated in which such high quality microlenses can be drawn from a shaped optical fiber preform. Figure 13 is a photograph of a shaped preform that has been fabricated by LLNL. In cross-sectional shape the fiber preform is ground so that it has the identical profile of that desired on the microlens although at a scale that is approximately 75 time larger in its transverse dimensions. In the pulling of the optical fiber from the preform the temperature is kept low enough so that the resulting fiber retains the desired cross-sectional shape of the preform. The final shaped-fiber diameter is approximately 350 microns yielding approximately 1 Km of fiber lens from the preform. After the lens is drawn it is cut into short 30 cm lengths and an AR coating is applied to both the input and output face. These coated lengths are then cut into 2 cm long pieces and individually attached to the LLNL diode packages.

Critical to obtaining good optical performance from the microlens conditioned packages is the flatness of the laser diode bar (absence of so called "smile") when it is attached to the top silicon surface of the LLNL package. Along the length of the diode bar (up to 1.8 cm) the flatness requirement is on the order of ± 1 micron. This flatness requirement is critical because of the short effective focal length of the microlenses. Our present generation lens shown in profile in Fig. 11 has an effective focal length of approximately 150 microns. This means that if the string of emitting apertures along the diode bar deviate from lying on a straight line by only 1.5 μm due to non planarity of the submount, then the resulting collimated diode radiation will be angularly deviated by 10 mRad which is the same as the far field beam divergence of the conditioned diode radiation. Since the silicon wafers used in the LLNL package production are polished on their surfaces this flatness requirement is

easily met. This is yet another advantage of the silicon processing technology that has been developed by LLNL; this flatness requirement is much harder to meet when using eithe.· BeO or copper as the submount material.

Figure 14 shows the coordinate system used in calculating the microlens' profile. The diode aperture is located at the origin of the coordinate system and rays of light leaving the origin are parameterized by the angle θ which they make with the x-axis. The flat input face of the lens is located at $x=a$, while the curved output face intersects the x-axis at $x=b$. Working in the first quadrant, the curved profile of the microlens denoted by the function $y=f(x)$ can be determined using a variational calculation based on Fermat's principle in which a ray is tracked from the origin through the lens to a focus point at infinity. As shown in the following derivation the desired surface of the optic is complicated but easily calculated numerically. To this end a coupled system of linear differential equations is derived in which the lens profile is described parametrically in terms of θ by the coordinate pair $(x(\theta),y(\theta))$.

A ray launched from the origin intersects the flat input face of the lens at the point (x_1,y_1) given by,

$$\begin{aligned} x_1 &= a \\ y_1 &= a \cdot \tan(\theta) \end{aligned} \tag{0.1}$$

Calling n the index of refraction of the lens material, the angle θ' in Fig. 13 is determined from Snell's law,

$$\sin(\theta) = n \cdot \sin(\theta'). \tag{0.2}$$

If the intersection of this ray with the curved surface of the lens is now denoted by (x,y) then the constraint placed on (x,y) by the slope of the ray inside the lens is,

$$\frac{y - a \cdot \tan(\theta)}{x - a} = \tan(\theta'). \tag{0.3}$$

Using (0.2) to eliminate θ' from (0.3) gives,

$$\frac{y - a \cdot \tan(\theta)}{x - a} = \frac{\sin(\theta)}{\sqrt{n^2 - \sin^2(\theta)}} \tag{0.4}$$

Calling d the optical path length of this ray from the origin to infinity, d is given by,

$$d = a\sqrt{1 + \tan^2(\theta)} + n\sqrt{(x-a)^2 + (y - a \cdot \tan(\theta))^2} + \sqrt{(x_\infty - x)^2 + (y - a \cdot \tan(\theta))^2} \tag{0.5}$$

Approximating the last radical in (0.5) by $x_\infty - x$ gives,

$$d = a\sqrt{1 + \tan^2(\theta)} + n\sqrt{(x-a)^2 + (y - a \cdot \tan(\theta))^2} + x_\infty - x. \tag{0.6}$$

Equations (0.4) and (0.6) represent two fundamental design equations for the lens surface $y=f(x)$. Fermat's principle requires that all rays that start at the origin and end at the focus at infinity have equal optical path lengths. Treating x and y in eqs (0.4) and (0.6) as functions of the parametric variable θ and implicitly differentiating with respect to θ leads to a coupled set of linear equations in $dx/d\theta$ and $dy/d\theta$,

$$\begin{pmatrix} (x-a)-\frac{1}{n}\sqrt{(x-a)^2+(y-a\cdot\tan(\theta))^2} & y-a\cdot\tan(\theta) \\ \frac{-(y-a\cdot\tan(\theta))}{(x-a)^2} & \frac{1}{x-a} \end{pmatrix}\begin{pmatrix} \frac{dx}{d\theta} \\ \frac{dy}{d\theta} \end{pmatrix} = \begin{pmatrix} \frac{-1}{n}\frac{a\cdot\sin(\theta)}{\cos^2(\theta)}\sqrt{(x-a)^2+(y-a\cdot\tan(\theta))^2}+(y-a\cdot\tan(\theta))\frac{a}{\cos^2(\theta)} \\ \frac{a}{(x-a)\cos^2(\theta)}+\frac{n^2\cos(\theta)}{(n^2-\sin^2(\theta))^{3/2}} \end{pmatrix} \quad (0.7)$$

In deriving (0.7), Fermat's principle has been invoked by setting $dd/d\theta=0$ when performing the differentiation in (0.6). Using the initial condition that at $\theta=0$, $x=b$ and $y=0$ it is a simple numerical calculation to generate the form of the curved lens surface. In this calculation the working distance a of the lens (see Fig. 13) is treated as a constant. Large numerical aperture diffraction limited lens profiles can be calculated by incrementally stepping through the angle θ and calculating the x and y values at each value of θ using (0.7) and the x and y values at the previous θ.

Conclusion

A modular, actively cooled laser diode array heatsink has been developed utilizing microchannel cooling technology. The heatsink enables high duty factor or even cw operation of fully filled semiconductor laser diode arrays at high average power. Using laminar flow the LLNL package enables a very low thermal impedance that is inherently efficient in terms of the hydraulic power needed to circulate the cooling fluid. The low thermal impedance enhances diode reliability by enabling diodes to run at low temperature. Reliability is also enhanced by the simplicity of the thermal circuit used in the LLNL package; only one solder connection is placed between the diode bar and the cooling fluid. The LLNL package was developed for use in pumping solid state lasers and as such enables very compact and lightweight DPSSL systems. The package's modularity and the minimization of external hydraulic and electrical connections has very much simplified the integration of semiconductor laser diode pump arrays into DPSSL systems, especially those having constrained weight and volume budgets. The simplicity of the stacking procedure used to build up two dimensional apertures enhances the flexibility of the LLNL approach as arbitrarily sized arrays can all be constructed using the same basic technology. Ease of manufacturability and holding down packaging costs have been key considerations in the development of the LLNL package. These points have been addressed by constructing the package from low cost silicon and glass and taking

advantage of previously well developed silicon processing technologies in the package fabrication. Holding the level of diode integration to only 1.8 cm of bar length per package enhances the maintainability of large two-dimensional arrays as it is a simple and inexpensive procedure to go in and remove a single non working package from a large array and replace it with a new one. Finally, two new LLNL developed technologies, optical conditioning using cylindrical microlenses and the efficient delivery of the output radiation from large optically conditioned two-dimensional diode arrays to rod lasers using lensing ducts, offers for the first time an inexpensive and commercially attractive diode end-pumping technology that is simply and easily scaled in average power. This technology has been demonstrated by LLNL in a Nd:YLF laser oscillator and a wing pumped Cr:LiSAF laser. Using this technology LLNL is pursuing a 2 μm Tm:YAG laser for medical applications as well as a high average power 1 μm Yb:YAG laser for material processing applications.

We appreciate and thank W. Krupke, G. Albrecht, B. Comaskey, P. Reichert, and E.V. George of Lawrence Livermore National Laboratory for many useful and stimulating discussions ducring the course of this work. Additionally, for their technical contribution to this work, the authors wish to express their appreciation and thanks to V. Sperry, T. Rodriguez, L. DiMercurio, E. Utterback, D. VanLue, C. Reinhardt, and D. Luna. This research was performed under the auspices of the U.S. Department of Energy by Lawrence Livermore National Laboratory under contract W-7405-Eng-48.

Figure Captions

1. Photograph of the LLNL microchannel cooled laser diode package.
2. a) Exploded view of the LLNL microchannel cooled package showing the three laminations used in its construction. b) Cross-sectional view of package.
3. Scanning electron microscope photograph of the microchannel region in the packages top silicon layer.
4. The three layers of a microchannel cooler package are shown along the top row. The features in the silicon microchannel and manifold layers are fabricated using an anisotropic etching technique while the features in the glass layer are fabricated using an ultrasonic milling technique. The bottom row shows the two silicon wafers and the single glass wafer that are used in the manufacture of the cooler assemblies.
5. a) Photograph of the LLNL package with its matching conductive silicone elastomer gasket. b) A single screw is used to locate individual packages and conductive silicone elastomer gaskets in an alternating sequence in the construction of large 2-dimensional diode arrays.
6. a) A 2-dimensional diode array for pumping a Nd:YAG slab laser. This array consists of 148 individual LLNL packages. The single water inlet and outlet to the stack are visible on the back of the array at either end. The two metal blocks are the positive and negative electrodes of the series connected stack. b) The Nd:YAG zigzag slab laser which is pumped by the diode array.
7. The improvements in average power scaled to a linear cm of bar material that have been demonstrated by LLNL over the last 4 years.
8. An L-I curve demonstrating a cw output power of 96 W from 1 linear cm of LLNL produced laser diode bar material.
9. Lifetest data in which a 1 cm long diode bar was run at a constant 22.2 W cw. The plot shows the drive current that was required to keep the bar at this cw output power as a function of elapsed time.
10. Theoretical maximum power output (right side axis) of a 1 cm bar with optimized output coupler reflectivity versus cavity length for material with losses of 5 cm^{-1} and 1 cm^{-1}. The thermal power dissipated in the bar when it is running cw at 28 °C above the cooling water in a microchannel cooler is also indicated (left side axis). This line is calculated using the measured thermal impedance value of 0.014 °C-cm^2/W for the LLNL package.
11. Cross-sectional view of a LLNL laser diode package with a conditioning microlens attached.
12. a) Schematic diagram of the LLNL end-pump architecture applied to a Nd:YLF Q-switched laser oscillator. b) Photograph of a lensing duct that was used to deliver pump radiation to a Cr:LiSAF laser rod.
13. Photograph of a shaped lens preform from which large numerical aperture diffraction limited cylindrical microlenses are fabricated using a fiber pulling technique.
14. Coordinate system used in calculating the profile of cylindrical microlenses for conditioning the optical output of laser diode arrays. The emitting diode aperture is located at the origin in this figure.

[1]R. Beach, W. Benett, B. Freitas, D. Mundinger, B. Comaskey, R. Solarz, and M. Emanuel, "Modular Microchannel Cooled Heatsinks for High Average Power Laser Diode Arrays," IEEE J. Quantum Electron., **28**, 966 (1992).
[2] W.J. Benett, B.L. Freitas, D. Ciarlo, R. Beach, S. Sutton, M. Emanuel, and R. Solarz, "Microchannel cooled heatsinks for high average power laser diode arrays," SPIE Vol. 1865, p 144 (1993).
[3]T.J. Bland, R.E. Niggemann, and M.B. Parekh, "A Compact High Intensity Cooler (CHIC)," SAE Technical Paper Series, Thirteenth Intersociety Conference on Environmental Systems, San Francisco, California July 11-14, 1983.
[4]D. Tuckerman and R. Pease, "High-Performance heatsinking for VLSI," IEEE Electron. Device Lett., vol EDL-2, p. 126, 1981.
[5]D. Tuckerman, "Heat-transfer microstructures for integrated circuits," Ph.D. dissertation, Stanford University, Stanford, CA., (1984).
[6]R.J. Phillips, "Microchannel Heat Sinks," The Lincoln Laboratory Journal, Volume 1, Number 1, p. 31 (1988).
[7]G. Wallis and D. Pomerantz, "Field assisted glass-metal sealing," J. Appl. Phys., vol 40, p. 3946, 1969.
[8] J.G. Endriz, M. Vakili, G.S. Bowder, M.A. DeVito, J.M. Haden, G.L. Harnagel, W.E. Plano, M. Sakamoto, D.F. Welch, S. Willing, D.P. Worland, and H.C. Yao, "High Power Diode Laser Arrays," IEEE J. Quantum Electron., **28**, 952 (1992).
[9] R.G. Waters, R.J. Dalby, J.A. Baumann, J.L. Sanctis, and A.H. Shepard, "Dark-Line-Resistant Diode Laser at 0.8 microns Comprising InAlGaAs Strained Quantum Well," IEEE Phot. Tech. Lett., 3, 409 (1991).
[10]J.J. Snyder, P. Riechert, and T. Baer, Appl. Opt. **30**, 2743 (1991).
[11]R. Beach, P. Reichert, W. Benett, B. Freitas, S. Mitchell, S. Velsko, J. Davin, R. Solarz, "Scalable diode-end-pumping technology applied to a 100-mJ Q-switched Nd^{3+}:YLF laser Oscillator," Optics Letters 18, 1329 (1993).
[12]M.D. Perry, S.A. Payne, T. Ditmire, R. Beach, G.J. Quarles, W. Ignatuk, R. Olson, and J. Wetson, "Better materials trigger Cd:LiSAF laser development," *Laser Focus World*, p 85 (September 1993).
[13]W.F. Krupke and L.L. Chase, Proc. Soc. Photo_Opt. Instrum. Eng. **1040**,68 (1989).
[14]P. Lacovara, H.K. Choi, C.A. Wang, R.I. Aggarwal, and T.Y. Fan, "Room-temperature diode-pumped Yb:YAG laser," Optics Letters 16, 1090 (1991).

Fig1

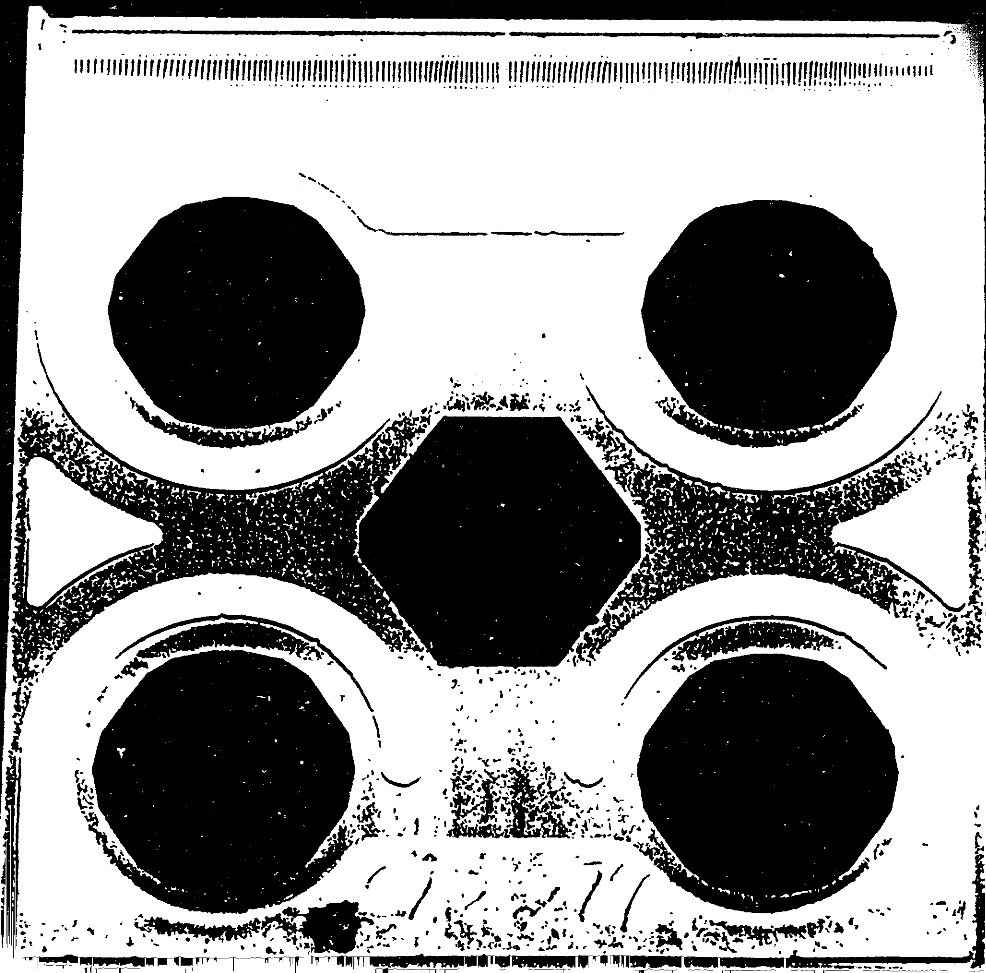

SKETCH NUMBER Fig 2

~~AA-ALT-0192-00~~

AA-ALT-0192 -007A

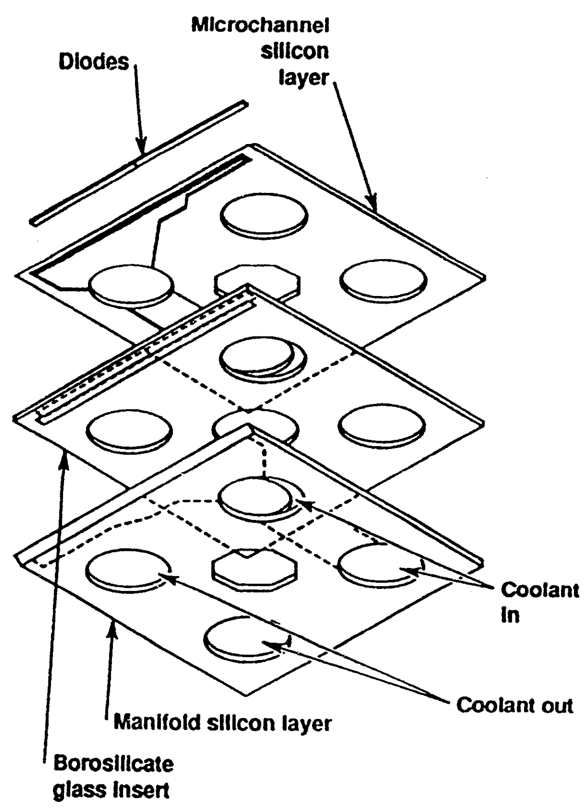

(a)

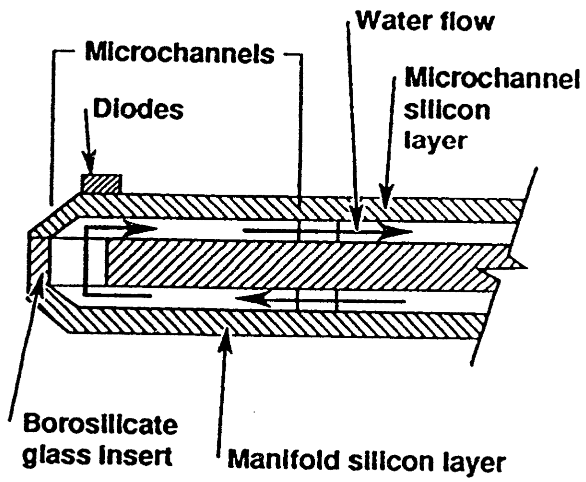

(b)

SKETCH

LAWRENCE LIVERMORE LABORATORY
UNIVERSITY OF CALIFORNIA

SUBJECT | DRAWN BY | DATE | BUILDING NO. | ROOM NO. | APPROVED BY | DATE

JOB ORDER INFORMATION: JOB NO. | SERIAL NO. | DATE ISSUED | DELIVER TO | TAG NO. | NO. REQD. | DATE REQD.

-112 (REV.8 71)

SKETCH NUMBER Fig 3

99-50-0193-0003

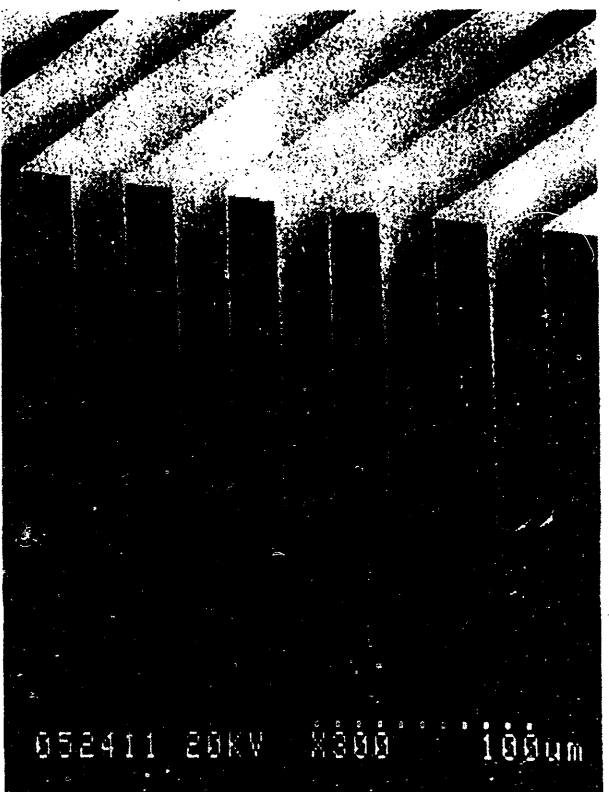

SKETCH

LAWRENCE LIVERMORE LABORATORY
UNIVERSITY OF CALIFORNIA

SUBJECT			
DRAWN BY		APPROVED BY	DATE
DATE	BUILDING NO.	ROOM NO.	

JOB ORDER INFORMATION			
JOB NO.		TAG NO.	
SERIAL NO.		NO. REQD.	
DATE ISSUED		DATE REQD.	
DELIVER TO			

12 (REV. 8-71)

SKETCH NUMBER Fig 4

99-50-1092-3257A

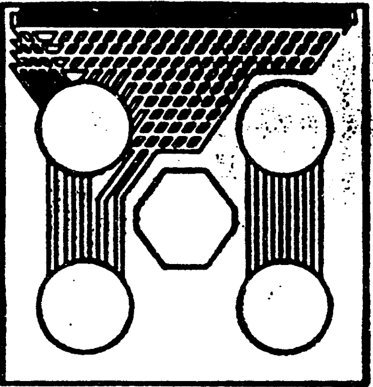

Microchannel layer

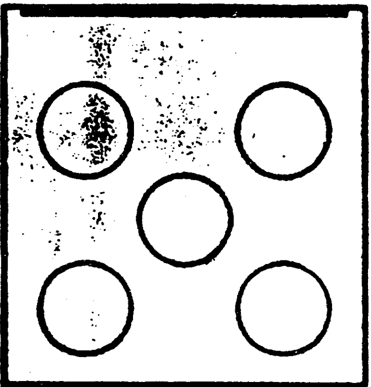

Glass Insert

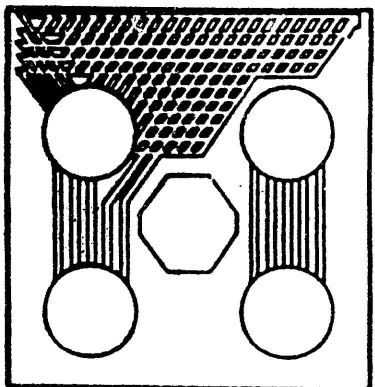

Manifold layer

SKETCH

LAWRENCE LIVERMORE LABORATORY
UNIVERSITY OF CALIFORNIA

SUBJECT	DRAWN BY	DATE	APPROVED BY	DATE	BUILDING NO.	ROOM NO.

JOB ORDER INFORMATION			
JOB NO.		TAG NO.	
SERIAL NO.		NO. REQD.	
DATE ISSUED		DATE REQD.	
DELIVER TO			

(REV.8 71)

SKETCH NUMBER Fig 5

99-50-0193-0028

SKETCH

LAWRENCE LIVERMORE LABORATORY
UNIVERSITY OF CALIFORNIA

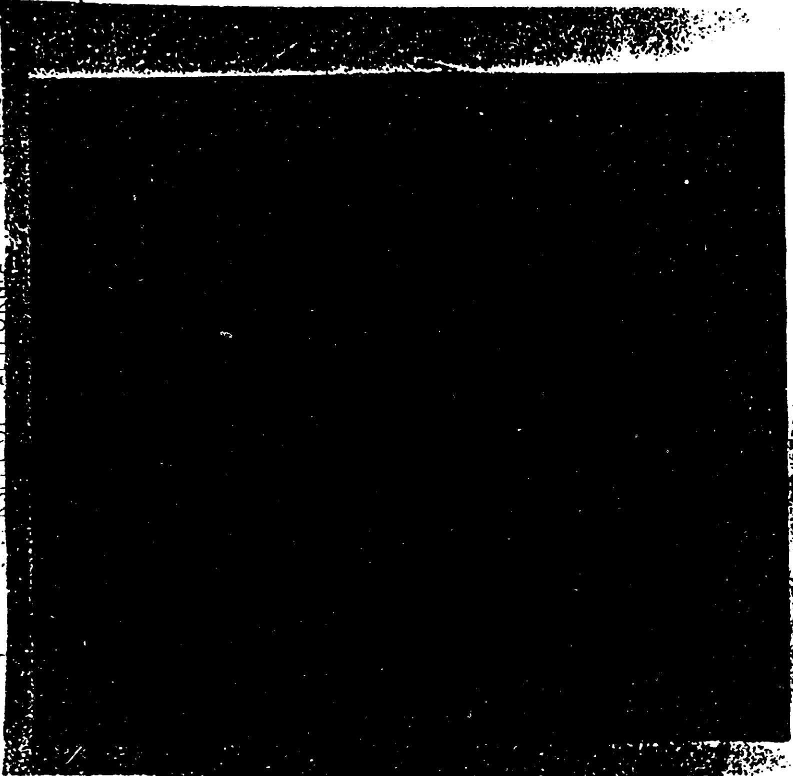

(a)

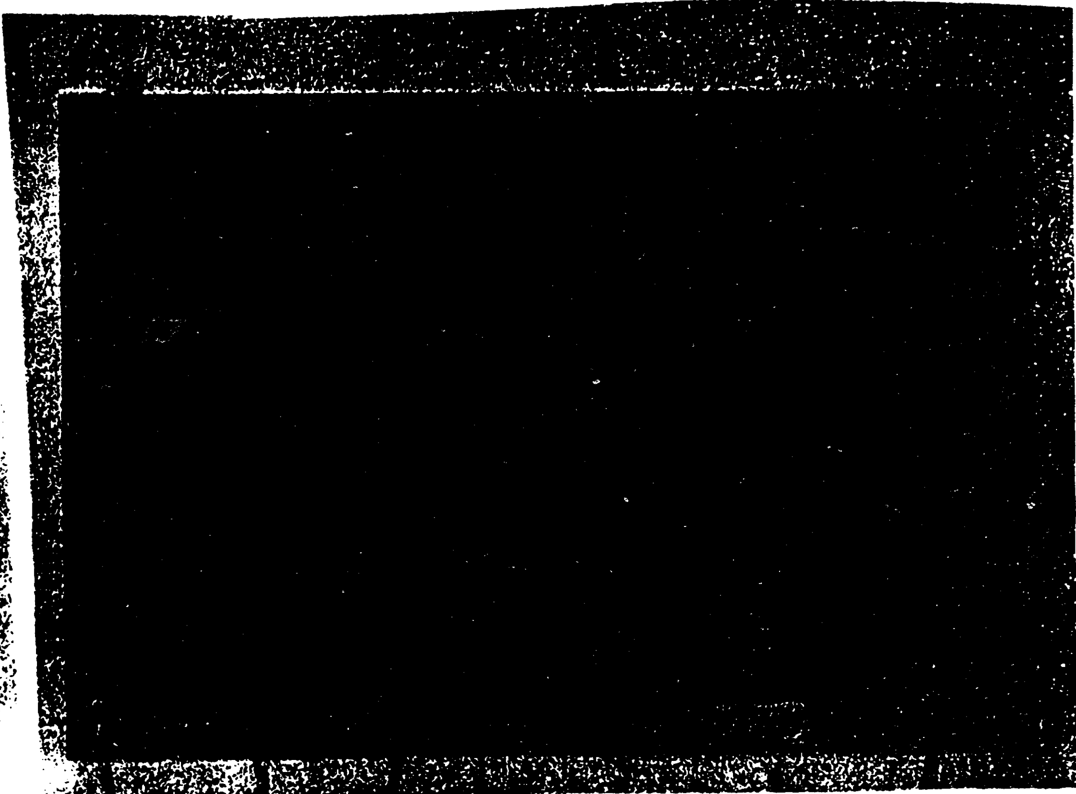

(b)

TAG NO.	JOB NO.
NO. REQD.	SERIAL NO.
DATE REQD.	DATE

ORDER INFORMATION

SUBJECT

DRAWN BY

DATE

BUILDING NO.

Fig 6a

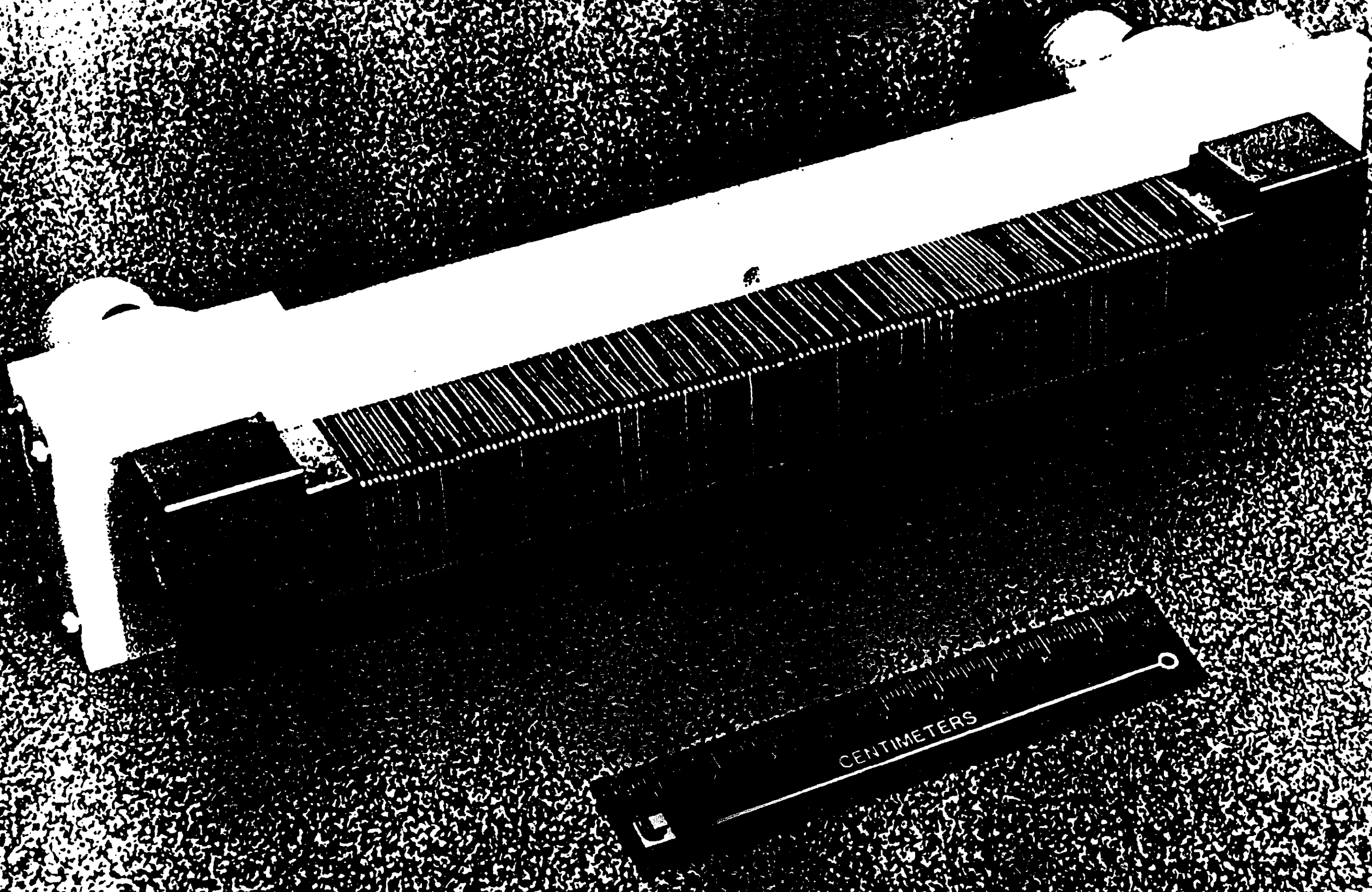

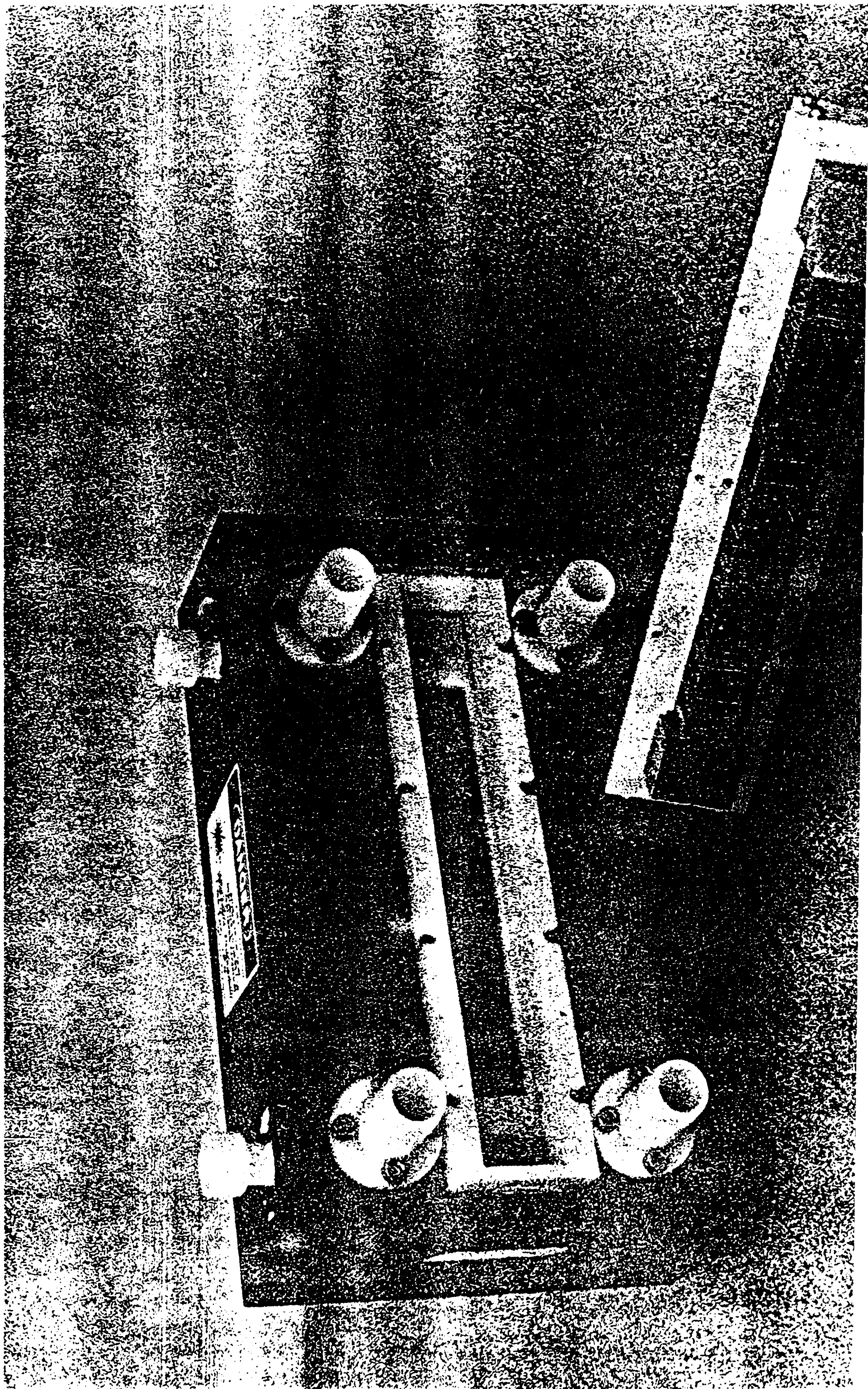

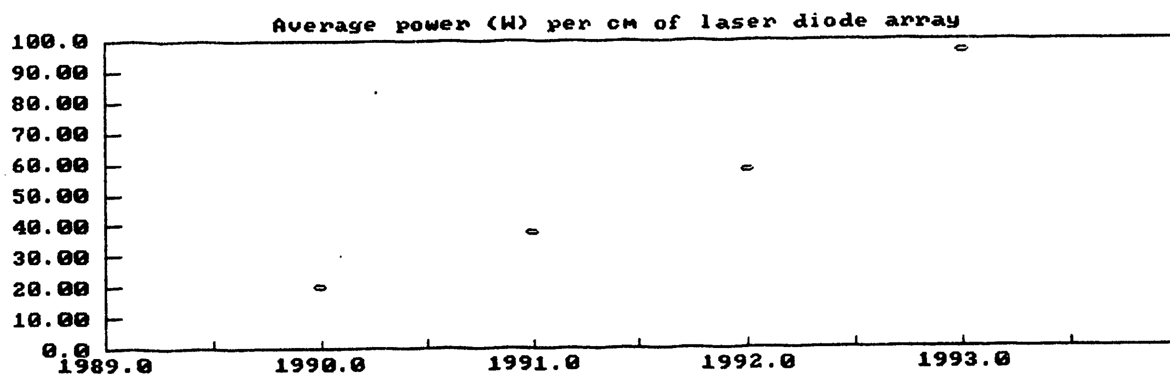

Fig 7

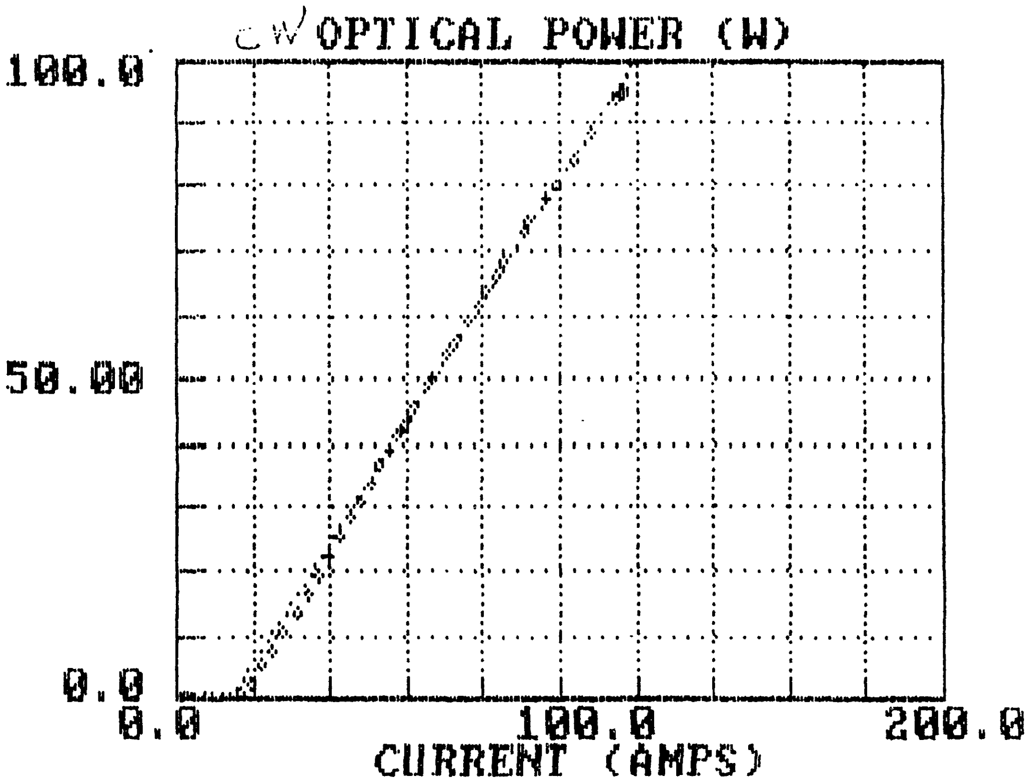

SKETCH

LAWRENCE LIVERMORE LABORATORY
UNIVERSITY OF CALIFORNIA

SUBJECT		
DRAWN BY		
DATE	BUILDING NO.	ROOM NO.
APPROVED BY		DATE

JOB ORDER INFORMATION

JOB NO.		TAG NO.	
SERIAL NO.		NO. REQD.	
DATE ISSUED		DATE REQD.	
DELIVER TO			

SKETCH NUMBER

-112 (REV.8 71)

SUBJECT			SKETCH LAWRENCE LIVERMORE LABORATORY UNIVERSITY OF CALIFORNIA		JOB ORDER INFORMATION	JOB NO.	TAG NO.
DRAWN BY						SERIAL NO	NO. REQD.
						DATE ISSUED	DATE REQD.
DATE	BUILDING NO.	ROOM NO	APPROVED BY	DATE		DELIVER TO	

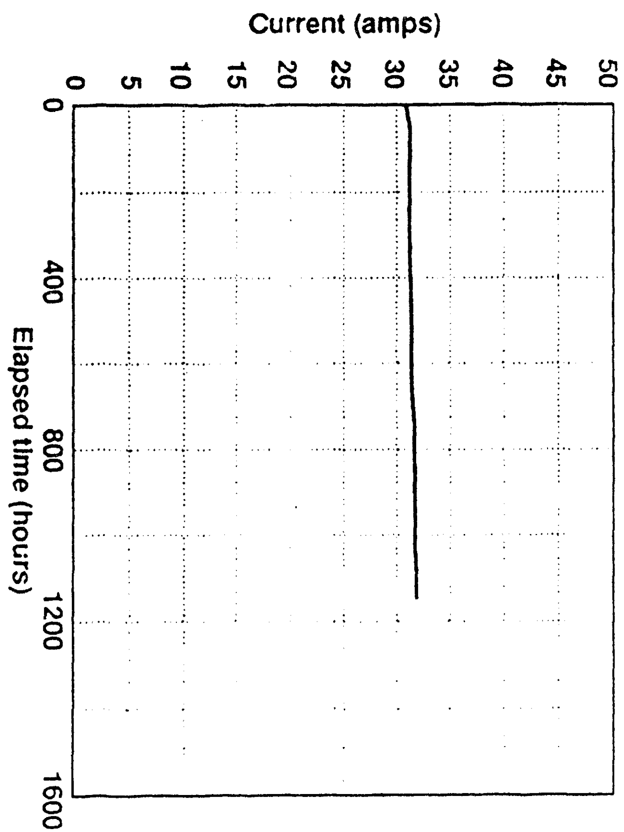

SKETCH NUMBER Fig 9

112 (REV 3 71)

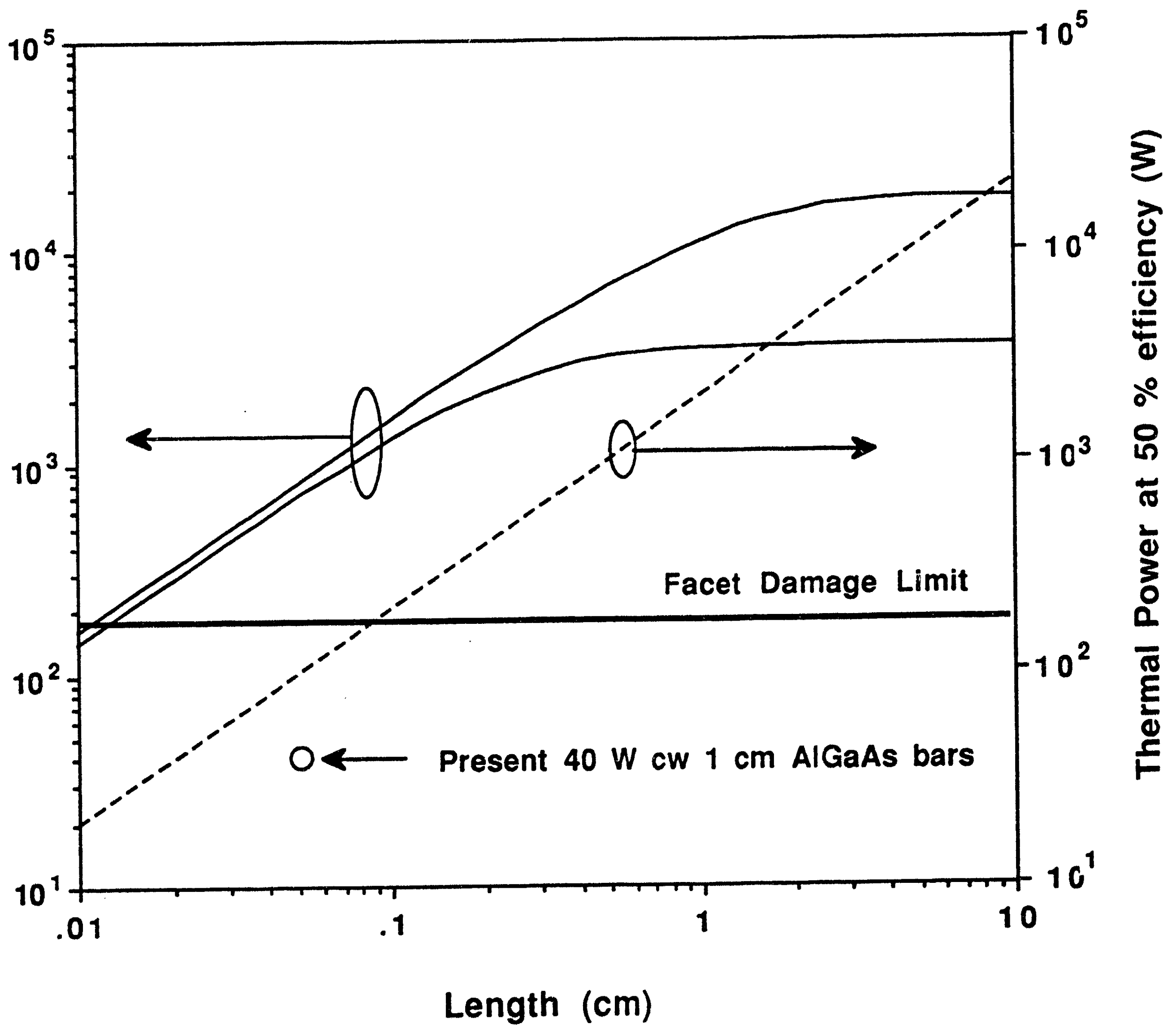

Fig. 1A

SKETCH

LAWRENCE LIVERMORE LABORATORY
UNIVERSITY OF CALIFORNIA

SUBJECT		JOB ORDER INFORMATION	JOB NO.	TAG NO
DRAWN BY			SERIAL NO	NO REQD.
DATE	BUILDING NO. / ROOM NO.	APPROVED BY / DATE	DATE ISSUED	DATE REQD.
			DELIVER TO	

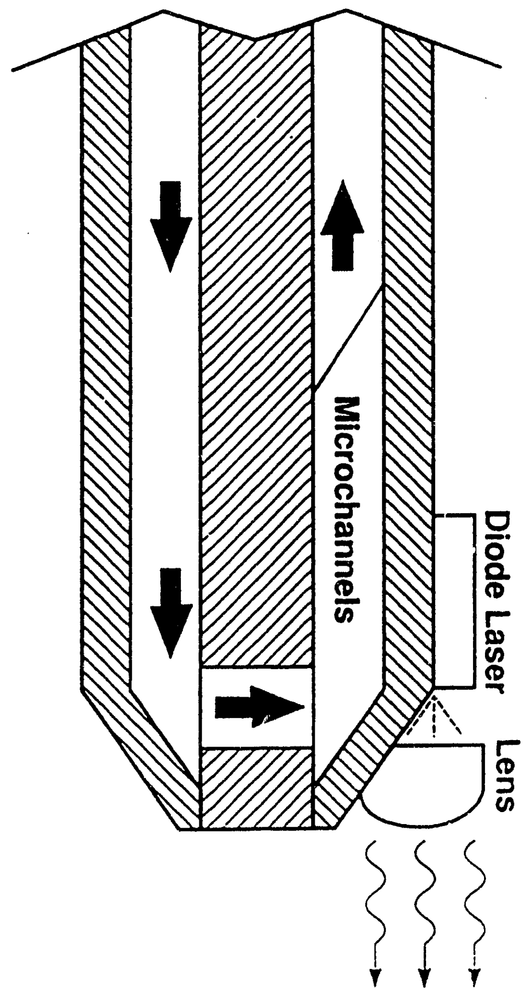

PRCLEO '93

SKETCH NUMBER Fig 10

-112 (REV.8 71)

SKETCH NUMBER Fig 12(a)

99-50-0192-0153C

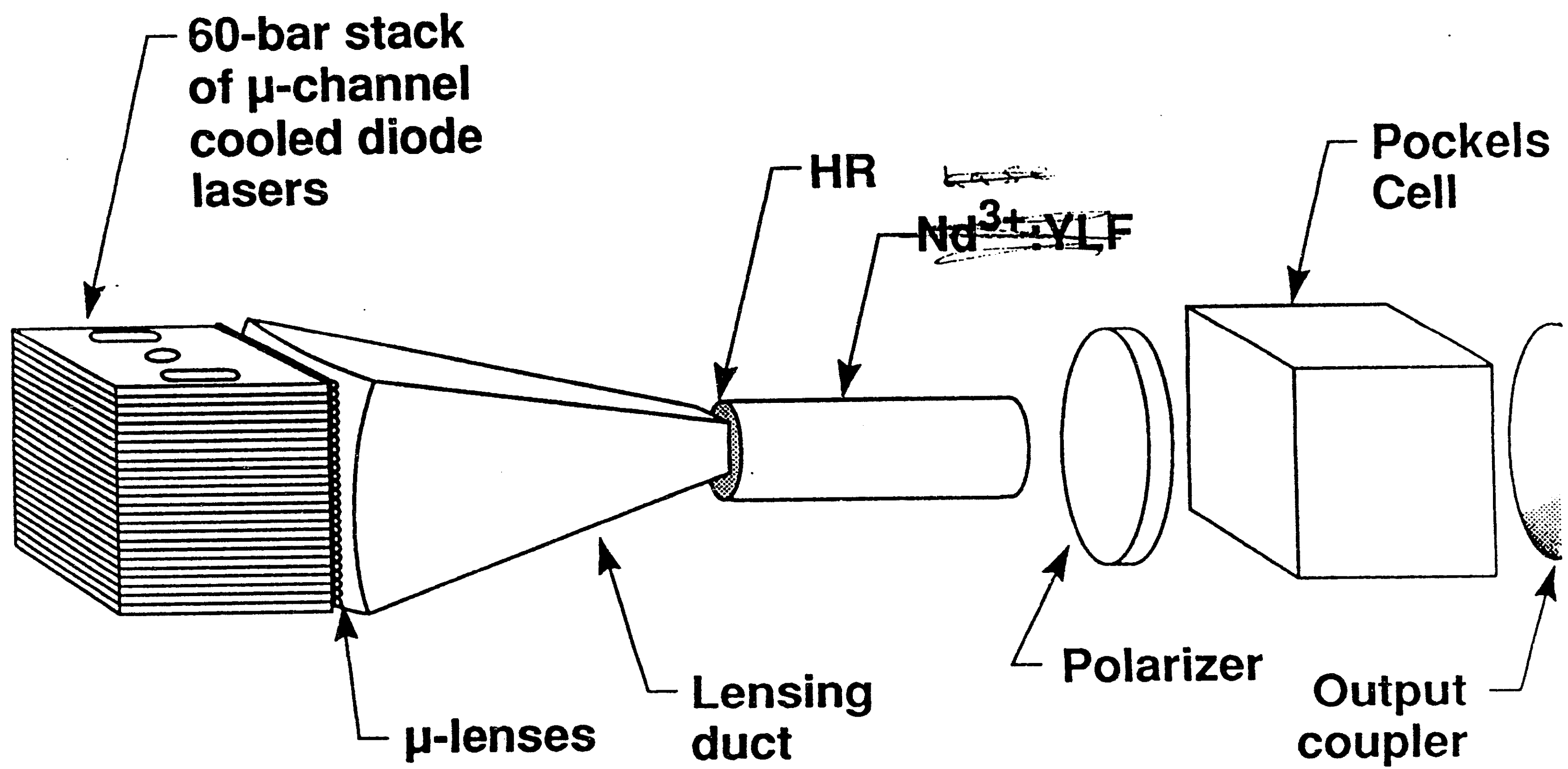

SKETCH
LAWRENCE LIVERMORE LABORATORY

94-50-1193-4355A Fig 12b

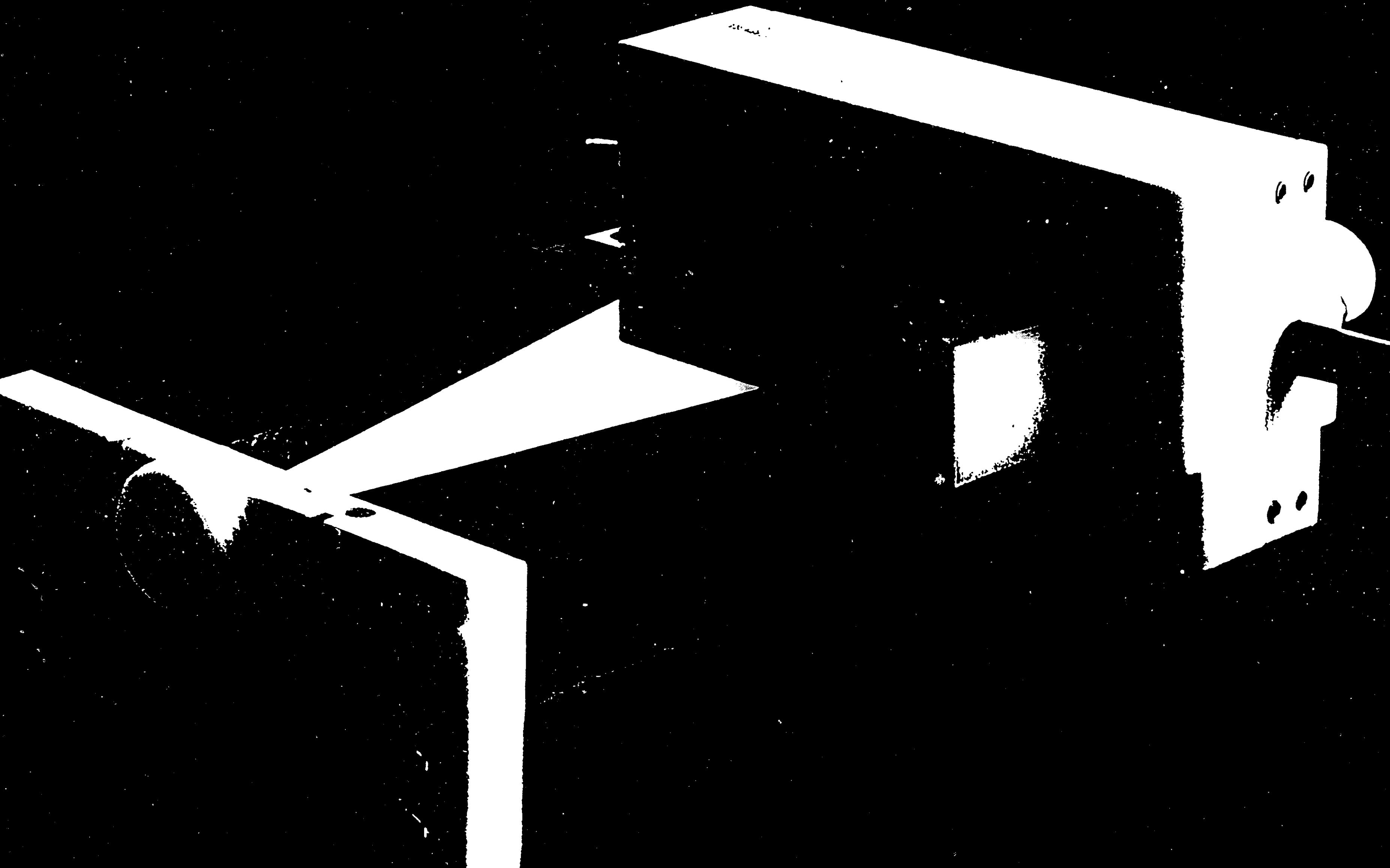

SUBJECT			SKETCH LAWRENCE LIVERMORE LABORATORY UNIVERSITY OF CALIFORNIA		JOB ORDER INFORMATION	JOB NO.	TAG NO.
DRAWN BY						SERIAL NO.	NO. REQD.
						DATE ISSUED	DATE REQD.
DATE	BUILDING NO.	ROOM NO.	APPROVED BY	DATE		DELIVER TO	

Shaped preform

SKETCH NUMBER Fig 12

L-112 (REV.8/71)

SUBJECT	SKETCH LAWRENCE LIVERMORE LABORATORY UNIVERSITY OF CALIFORNIA	JOB ORDER INFORMATION	JOB NO.	TAG NO.
			SERIAL NO.	NO. REQD.
DRAWN BY			DATE ISSUED	DATE REQD.
DATE / BUILDING NO. / ROOM NO.	APPROVED BY / DATE		DELIVER TO	

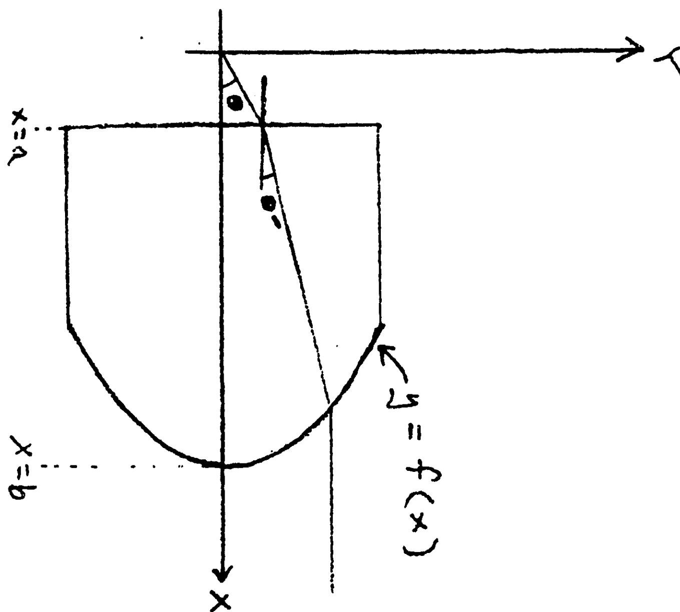

SKETCH NUMBER Fig 13

-112 (REV.8/71)

DATE FILMED

5/12/94

END